# Enhancements and validation of the real-time optimised D-Region HF radio absorption model


**Neil C. Rogers and Farideh Honary**

Space & Planetary Physics, Lancaster University, UK

Dr Neil C. Rogers

n.rogers1@lancaster.ac.uk


## 1: Introduction

The **Optimised D-Region Absorption Model (ODRAM)**[1,2] (Fig. 1) provides global nowcasts and forecasts of HF (3-30 MHz) radio wave absorption in the ionosphere. This results from ionisation by solar flares, magnetospheric electron precipitation (in auroral regions), and Solar Energetic Particles (SEP) in the polar cap. Parameters of ODRAM are optimised in near real time by assimilating satellite measurements, geomagnetic index estimates, and direct measurements of absorption made by riometers at high latitudes.

This poster describes enhancements to the individual model components and some results of model validation.

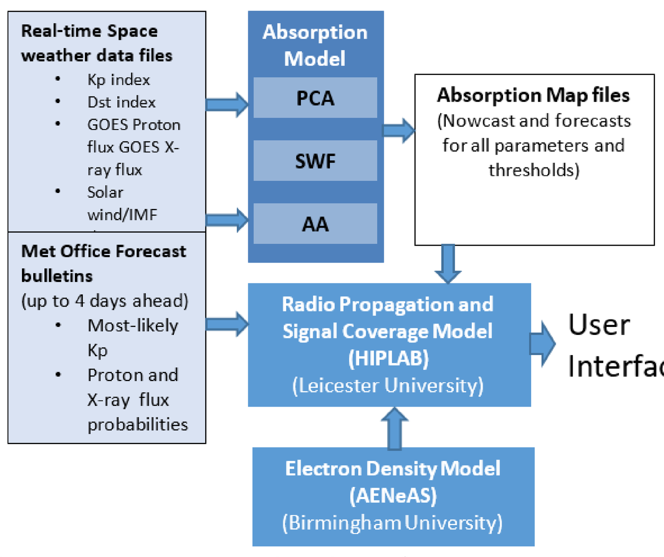


***Fig. 1.*** *ODRAM model data flow. PCA = Polar Cap Absorption, SWF = shortwave fadeout, AA = Auroral absorption.*

## 2: Measuring Absorption: The Global Riometer Array (GloRiA)

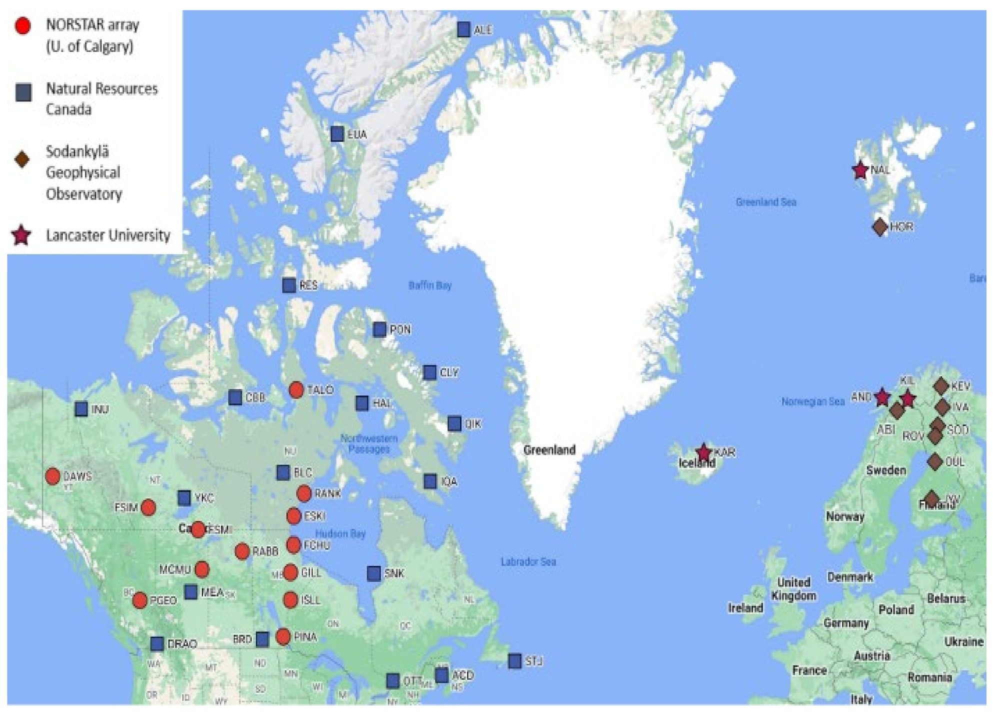


***Fig. 2.*** *Riometers from four institutions in GloRiA.*

Riometers measure **30 MHz cosmic noise absorption (CNA)** in the ionosphere by reference to a "Quiet Day Curve" recorded in a recent period of low space weather activity. They comprise a horizontal crossed-dipole antenna, narrowband receiver, and calibration noise source.

The GloRiA collaboration aims to resolve issues around data sharing, licensing, common data formats and processing, and intercalibration of riometers.

| |
|---|
| **AndøyaSpace, Norway,** |
| **British Antarctic Survey (BAS)** |
| **Lancaster University, UK** |
| **Natural Resources, Canada (NRCan)** |
| **Polar Research Institute of China (PRIC),** |
| **Sodankylä Geophysical Observatory, Finland, (SGO)** |
| **South African National Space Agency (SANSA),** |
| **University of Calgary, Alberta, Canada** |

***Table 1**. GloRiA participants*

## 3: Shortwave Fadeout Models (Solar Flares)

Shortwave Fadeout (SWF) describes HF radio wave absorption due to photoionisation of the D-region ionosphere during solar flares. It correlates closely with the 0.1–0.8nm solar X-ray flux ($F_x$) with a lag of 1–10 minutes[3] and depends on solar-zenith angle, $\chi$. ODRAM initially adopted the SWF model $A_{DRAP}$ used in the NOAA D-RAP product[4,5]

Table 2 (col. 1) defines $A_{DRAP}$, a new model, $A_{Fiori}$ by Fiori *et al.* (2022)[6] based on 87 flares in the Solar Cycle 24, and an early model $A_{Sato}$ by Sato, (1975)[7] based on 15 flare events. All models are based on riometer observations of CNA.

We assessed these models using a database of all 126 X-class flares in Solar Cycle 23, with CNA from riometers in the NORSTAR and SGO arrays and the KIL riometer at Kilpisjärvi, Finland (KIL) (Fig. 2). Times of SEP events, night-time, and radio interference (CNA < 0.1 dB) were excluded, as were riometers in the principal region of auroral absorption (62°-68° invariant latitude).

| Model (dB) | MPE (%) | MPE (%) CNA >1dB | PE | PE CNA >1dB |
|---|---|---|---|---|
| $A_{DRAP} = 0.5\left((10\log F_x + 65)\cos^{0.75}(\chi)/f\right)^{1.5}$ | -70 | -85 | -0.357 | -3.345 |
| $A_{Fiori} = 12{,}080\, F_x \cos\chi$ | +1.2 | +59 | -1.670 | -6.936 |
| $A_{Sato} = 4370\sqrt{10^3 F_x}\cos(\chi)/f^2$ | +28.3 | -6.5 | 0.526 | 0.372 |
| $A_{Rogers1} = \mathbf{4774}\, F_x(\cos\chi)^{\mathbf{0.87}}$ | -54 | -31 | 0.440 | -0.032 |
| $A_{Rogers2} = \mathbf{131.8}\sqrt{F_x}\cos\chi$ | +10.1 | -19.7 | 0.565 | 0.189 |
| $A_{Rogers3} = \mathbf{92.4}\sqrt{F_x}(\cos\chi)^{\mathbf{0.503}}$ | +30.5 | -20.5 | 0.620 | 0.267 |

***Table 2:*** *Parameters, Mean percentage errors (MPE), and Prediction Efficiency (PE) for six SWF models. $F_x$ is in Wm$^{-2}$. $f$ is the radio frequency (MHz) (30 MHz where not stated). Coefficients in bold were determined by regression.*

Plots of modelled *vs.* measured CNA during flares are presented in Fig. 3a-c for $A_{DRAP}$, $A_{Fiori}$ and $A_{Sato}$ respectively. The mean percentage error (MPE) and Prediction Efficiency (PE) of each model is presented in Table 1, including values for a subset of CNA values > 1dB which characterise model performance during strong SWF events. **The $A_{DRAP}$ SWF model has a strong negative bias**, which has been noted in the recent literature[8,6,9,10]. The $A_{Fiori}$ model has a positive bias at high values of CNA (>1dB) but is relatively unbiased overall. **$A_{Sato}$ is the only one of the three published models with a positive PE and has only a small negative bias for CNA > 1dB.**

Three further models, ($A_{Rogers\,1,2,3}$ in Table 2, and d,e,f in Fig. 3) were developed and optimised by regression to our Solar Cycle 23 measurements. Parameterisation by $\sqrt{F_x}$ rather than $F_x$ has a better physically justification (Sato, 1975[7]) and results in improved model performance. Optimising the exponent on the $\cos\chi$ term provides marginal improvement to PE, but worsens the MPE.

In conclusion, we would recommend Sato's model as it combines high PE with low MPE for large CNA values, which are of greatest operational importance.

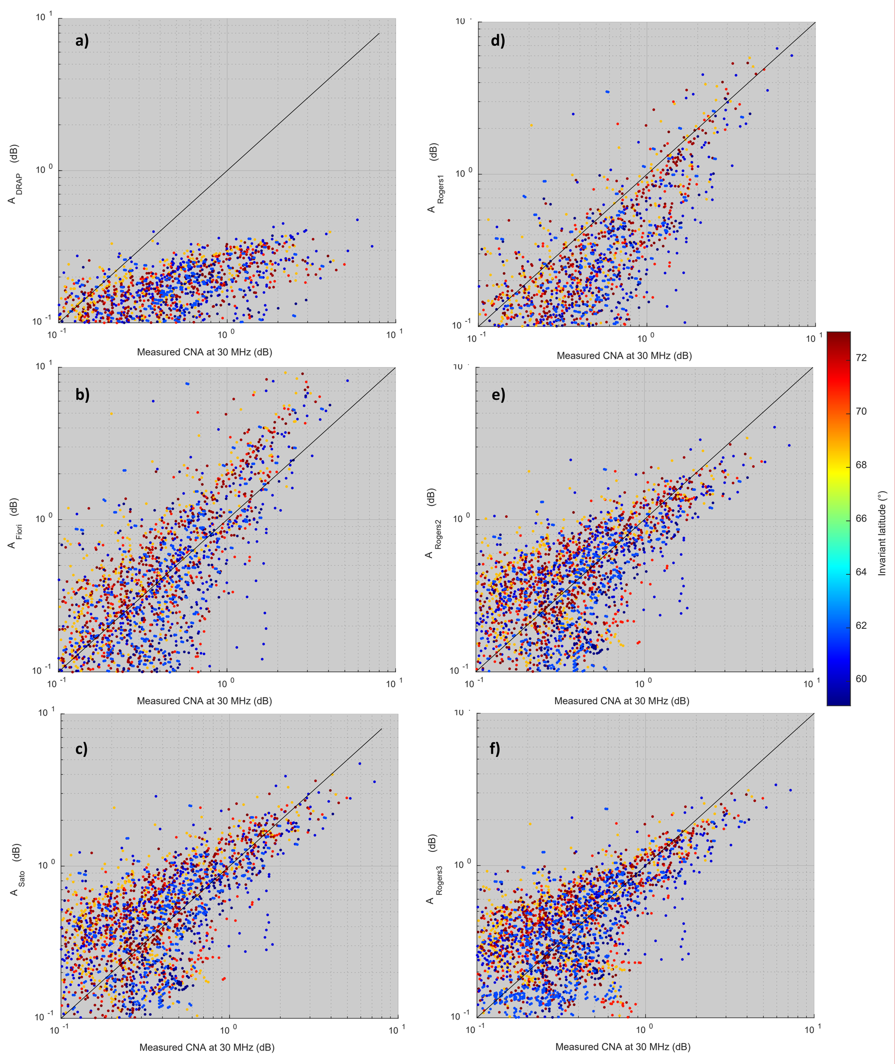

***Fig. 3.*** *Six models vs. measured CNA at 30 MHz for solar flare times in Solar Cycle 23.*

## 4: Auroral Absorption Models (Magnetospheric electrons)

The real-time Auroral Absorption (AA) model in ODRAM can be selected as either the of Foppiano & Bradley model[11] (an ITU-R standard for HF communications) or a new empirical model parameterised by geomagnetic latitude, magnetic local time (MLT) and a driver parameter – a geomagnetic index or a proxy derived from solar wind and interplanetary magnetic field measurements time-shifted to the bow shock nose[12].

The new models are developed from CNA recorded on 13 NORSTAR riometers, eight SGO riometers, and the KIL (Kilpisjärvi, Finland) riometer (Fig. 2), recorded throughout Solar Cycle 23. Periods of geomagnetic sudden commencements, SEP events, solar flares, and radio interference were excluded.

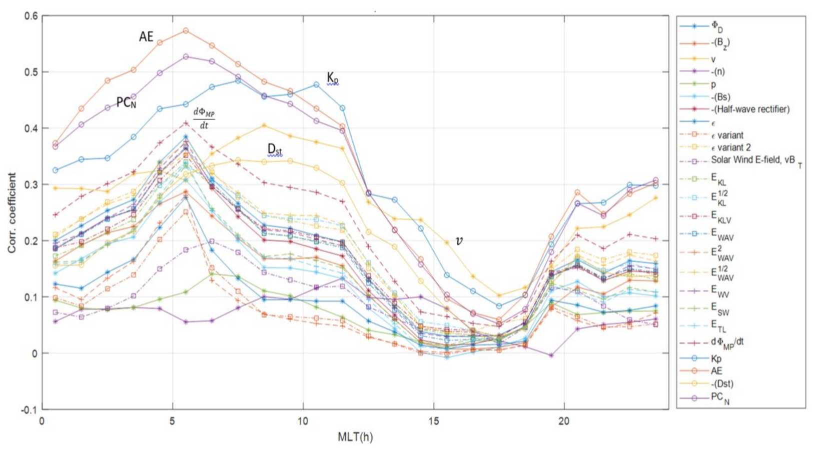

***Fig. 4.*** *Correlation between Kilpisjärvi CNA and solar-wind-magnetosphere coupling functions and geomagnetic indices.*

Fig. 4 shows the correlation between the CNA at KIL and 21 solar-wind-magnetosphere coupling functions (defined in Newell et al. [13]) and four geomagnetic indices for 1-h ranges of MLT. Four of the best performing driver parameters ($K_p$, AE, *Newell et al.'s*[13] recommended solar-wind – magnetosphere coupling function $\frac{d\phi_{MP}}{dt}$, and the solar wind speed, $v$) have been developed into empirical models for ODRAM.

We found that averaging solar wind coupling functions over a 1-h period was optimal. An example of the median AA at KIL vs. (MLT, $K_p$) is shown in Fig. 5. We combined data from multiple riometers in 2° geomagnetic latitude bins (from 58° to 76°N) to produce 3-d lookup tables of the probabilities of exceeding 0.5 and 1 dB absorption, and the median auroral absorption, an example of which is shown in Fig 6. for $K_p$ = 5 – 6.

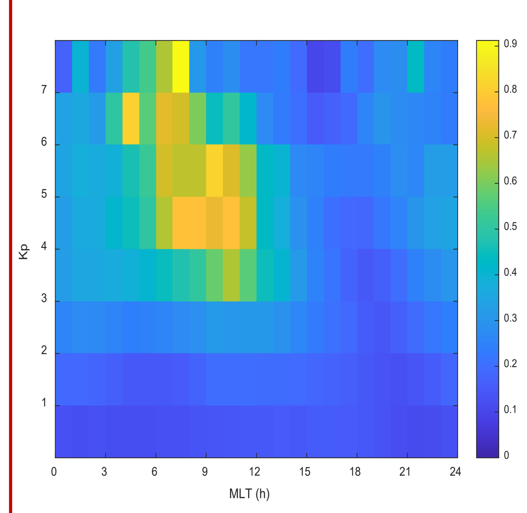

***Fig. 5.*** *Median AA at the KIL riometer vs. (MLT, $K_p$).*

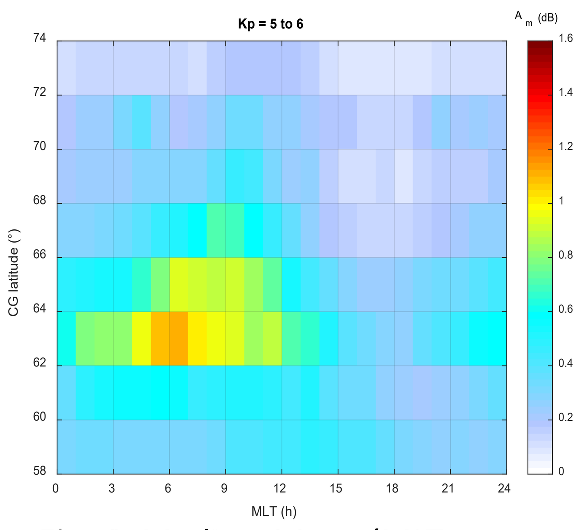

***Fig. 6.*** *Median AA vs. (MLT, geomagnetic latitude) for $5 \leq K_p < 6$*

## 5: Validation of Polar Cap Absorption Models (SEP events)

Real-time riometer data may be used in ODRAM to optimise coefficients of the PCA model[1,2], which can vary with changes in polar D-region composition, temperature, the hardness of the proton spectrum, or the rigidity cutoff boundary location. We have run tests for the active space weather period 4 – 16 September 2017, in which there were two SEP events, a succession of M and X-class flares, and a geomagnetic storm. The flux of > 10 MeV protons for the period is shown in Fig. 7.

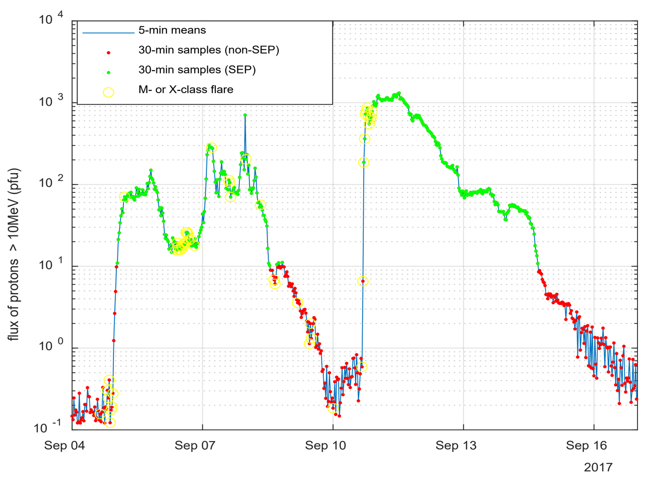

***Fig. 7.*** *Solar (>10 MeV) proton flux for Sep 2017. (Flare times indicated)*

We present one example in which ODRAM optimised PCA model coefficients $m_d$ and $m_n$ (the ratios of CNA to the square-root of proton flux above an energy threshold in the day and night respectively). Error metrics presented in Fig. 8 show that assimilating data from ten independent riometers (PGEO, JYV, ROV, IVA, FCHU, YKC, IQA, INU, CLY, and TALO) improved RMS error in 7/10 test riometers and improved bias in 8/10 test riometers. However, optimising with a single polar-cap riometer (TALO) can often reduce performance.

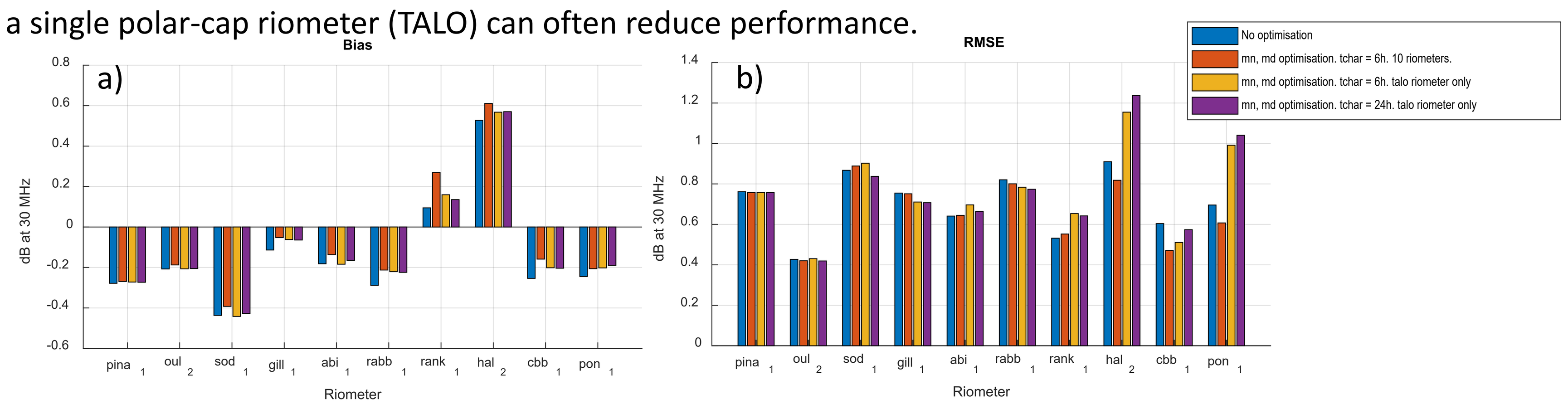

**Fig. 8.** *Performance metrics for four ODRAM simulations at 10 test riometer locations (in order of increasing geomagnetic latitude). a) RMSE, b) Bias.*

Other tests indicated that while including riometers from auroral latitudes aids the optimisation of the rigidity cutoff latitude boundary, they can bias the PCA model coefficients $m_d$ and $m_n$. Ideally, a polar-cap riometer should be included simultaneously for both the dayside and night ionospheres, but this is impractical under solstice conditions when all riometers are in the same (northern) hemisphere.

## 6: A 'Quiet-Day' model of absorption

The HF radio absorption models described above (and riometer measurements) indicate only the *increase* in absorption compared to a quiet day. To this must be added a small component of absorption due to diurnal and seasonal changes in the D-region chemistry, temperature, and solar illumination. We used a background 3-d model of *D* and *E*-region electron density called FIRI [14] determined from Faraday rotation measurements on sounding rockets, parameterised by the $F_{10.7}$ solar activity index. These were combined with neutral density and temperature profiles from the NRL MSIS 2.0 model to determine the complex refractive index (using Appleton's equation) and hence the absorption rate. Fig. 9 presents an example of quiet-day absorption predictions for 21 December. Deviative absorption is not included in this model due to its dependence on radio ray path trajectory and critical plasma frequencies (relative to $f$).

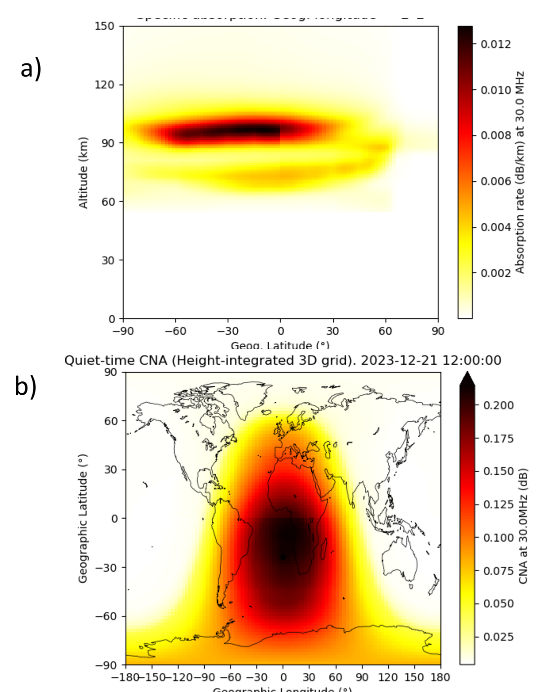

***Fig. 9.*** *Modelled quiet-day 30-MHz absorption (dB/km) at 12 GMT on 21 Dec., a) along 2°W meridian and b) height-integrated over the globe. $F_{10.7}$ = 75.*

## 7: Conclusions

- The Shortwave Fadeout (solar flare) model of HF radio absorption (currently the NOAA DRAP model) should be replaced by that of Sato (1975) [7].
- For a data-driven Auroral Absorption model, the driver parameters AE, $K_p$, Newell et al.'s 2007 coupling function or solar wind speed correlate best with 30 MHz absorption measurements in Solar Cycle 23.
- Moderate improvements to Polar Cap Absorption model performance are achieved when assimilating contemporary riometer measurements (CNA). However, issues of poor calibration and auroral absorption contamination need careful consideration.
- A climatological 'quiet-day' absorption model has been implemented to account for diurnal and seasonal variations in HF radio wave absorption.

## References


1. Rogers, N. C. & F. Honary, (2015) Assimilation of real-time riometer measurements into models of 30 MHz polar cap absorption. https://doi.org/10.1051/swsc/2015009
2. Rogers, N. C., et al. (2016) Improving the twilight model for polar cap absorption nowcasts. https://doi.org/10.1002/2016SW001527
3. Chakraborty, S., et al. (2021a) Ionospheric sluggishness: A characteristic time-lag of the ionospheric response to solar flares. https://doi.org/10.1029/2020JA028813
4. Schumer, E. (2009) *PhD Dissertation*, AFIT/DS/ENP/09-J01, U.S. Air Force, Wright-Patterson AFB, OH, USA. https://apps.dtic.mil/sti/tr/pdf/ADA516063.pdf
5. Sauer, H., & Wilkinson, D. C., (2008) Global mapping of ionospheric HF/VHF radio wave absorption due to solar energetic protons. https://doi.org/10.1029/2008SW000399
6. Fiori et al. (2022) Data-based optimization of a simple shortwave fadeout absorption model. https://doi.org/10.1016/j.jastp.2022.105843
7. Sato, T. (1975) Sudden $f_{min}$ Enhancements and Sudden Cosmic Noise Absorptions Associated with Solar X-Ray Flares. https://doi.org/10.5636/jgg.27.95
8. Chakraborty, S., et al. (2021b) A modeling framework for estimating ionospheric HF absorption produced by solar flares. https://doi.org/10.1029/2021RS007285
9. Nielsen, A. S., (2022) Validation of an empirical model of HF radio absorption during solar X-ray flares, *Masters Thesis.* https://apps.dtic.mil/sti/trecms/pdf/AD1173456.pdf
10. Levine, E. V., et al. (2019) A parameterized model of X-ray solar flare effects on the lower ionosphere and HF propagation. https://doi.org/10.1029/2018RS006666
11. Foppiano, A.J., & P.A. Bradley (1983) Prediction of auroral absorption of high-frequency waves at oblique incidence. handle.itu.int/11.1004/020.3000/ITU011-1983-10-en
12. King, J.H. & N.E. Papitashvili (2005) Solar wind spatial scales in and comparisons of hourly Wind and ACE plasma and magnetic field data. https://doi.org/10.1029/2004JA010649.
13. Newell, P. T., et al. (2007), A nearly universal solar wind-magnetosphere coupling function inferred from 10 magnetospheric state variables. https://doi.org/10.1029/2006JA012015
14. Friedrich, M., and K. M. Torkar (2001) FIRI: A Semiempirical Model of the Lower Ionosphere. https://doi.org/10.1029/2001JA900070



## Acknowledgements

This work was funded by the **Natural Environment Research Council** grant NE/V002686/1.

We are grateful to Sodankylä Geophysical Observatory, University of Oulu, and the NORSTAR riometer group at the University of Calgary for riometer data, the NOAA Space Weather Prediction Centre for GOES and ACE satellite data, and Kyoto University for geomagnetic indices.